Molecular Cancer Therapeutics

Targeted Delivery of Cytotoxic NAMPT Inhibitors Using Antibody–Drug Conjugates

Christopher S. Neumann[1], Kathleen C. Olivas[1], Martha E. Anderson[1], Julia H. Cochran[1], Steven Jin[1], Fu Li[1], Luke V. Loftus[1], David W. Meyer[1], Jason Neale[1], Jay C. Nix[2], Paul G. Pittman[1], Jessica K. Simmons[1], Michelle L. Ulrich[1], Andrew B. Waight[1], Abbie Wong[1], Margo C. Zaval[1], Weiping Zeng[1], Robert P. Lyon[1], and Peter D. Senter[1]

Abstract

Antibody–drug conjugates (ADCs) are a therapeutic modality that enables the targeted delivery of cytotoxic drugs to cancer cells. Identification of active payloads with unique mechanisms of action is a key aim of research efforts in the field. Herein, we report the development of inhibitors of nicotinamide phosphoribosyltransferase (NAMPT) as a novel payload for ADC technology. NAMPT is a component of a salvage biosynthetic pathway for NAD, and inhibition of this enzyme results in disruption of primary cellular metabolism leading to cell death. Through derivatization of the prototypical NAMPT inhibitor FK-866, we identified potent analogues with chemical functionality that enables the synthesis of hydrophilic enzyme-cleavable drug linkers. The resulting ADCs displayed NAD depletion in both cell-based assays and tumor xenografts. Antitumor efficacy is demonstrated in five mouse xenograft models using ADCs directed to indication-specific antigens. In rat toxicology models, a nonbinding control ADC was tolerated at >10-fold the typical efficacious dose used in xenografts. Moderate, reversible hematologic effects were observed with ADCs in rats, but there was no evidence for the retinal and cardiac toxicities reported for small-molecule inhibitors. These findings introduce NAMPT inhibitors as active and well-tolerated payloads for ADCs with promise to improve the therapeutic window of NAMPT inhibition and enable application in clinical settings. *Mol Cancer Ther; 17(12); 2633–42. ©2018 AACR.*

Introduction

Antibody–drug conjugates (ADCs) have attracted a great deal of recent interest, with FDA approval of four drugs and promising data from several others in various stages of clinical development (1). Most of the advanced ADCs contain antitubulin drugs such as auristatins and maytansines, or DNA-targeted drugs such as calicheamicins and camptothecins (2–5). While these payloads have been applied to a broad spectrum of tumor types, an important objective within the field has been to extend the technology beyond these drug classes and to identify novel agents that have complementary mechanisms of activity (1). This endeavor has proven to be quite challenging, because most drugs do not have the right profiles of potency, availability, chemical functionalities, and stability required for successful application as ADC warheads. Identification of new payloads will help advance this promising and rapidly advancing therapeutic modality.

We became interested in exploring inhibitors of nicotinamide phosphoribosyltransferase (NAMPT) as ADC payloads due to their chemical simplicity, high potencies on both their biochemical targets and on cells, and their unique mechanisms of activity (6). NAMPT is a key regulator of NAD levels in cells. In addition to serving as an essential redox cofactor to support energy and anabolic metabolism, NAD serves as a substrate for PARPs, sirtuins, and cyclic-ADP-ribose synthases (7). The nicotinamide byproduct from these enzymatic reactions is converted back into NAD via a salvage biosynthetic pathway involving NAMPT as the rate-limiting step. In this way, NAMPT maintains the NAD pool at a level sufficient to support metabolism. When NAMPT is inhibited, NAD levels decline below the level needed for metabolism leading to energy crisis and ultimately cell death. In contrast to many other cytotoxic molecules, the cell death following depletion of NAD proceeds via a nonapoptotic and proinflammatory mechanism termed oncosis (8). These mechanisms of action and cell death distinguish NAMPT inhibitors from current ADC payloads.

In addition, nontargeted small-molecule NAMPT inhibitors advanced to clinical trials but gave disappointing results. Clinical candidates FK-866, CHS-828, and GMX-1777 each encountered dose-limiting toxicities prior to any objective responses (9–11). More recent efforts to advance NAMPT inhibitors as small molecules appear to have met with unsuitable retinal and cardiac toxicities in preclinical species (12, 13), and there are no NAMPT inhibitors approved for clinical use at this time. We envisioned that a delivery approach using ADCs might circumvent the toxicities observed with systemic administration of NAMPT inhibitors, thus enabling the successful use of this drug class in the clinic (14). Here, we report that ADCs comprising NAMPT inhibitors (NAMPTi-ADCs) kill cells in an antigen-specific manner through depletion of intracellular NAD pools, and that the resulting conjugates display significant levels of activity in several tumor models at well-tolerated doses.

[1]Seattle Genetics, Inc., Bothell, Washington. [2]Advanced Light Source, Lawrence Berkeley Laboratory, Berkeley, California.

Note: Supplementary data for this article are available at Molecular Cancer Therapeutics Online (http://mct.aacrjournals.org/).

Corresponding Author: Christopher S. Neumann, Seattle Genetics, Inc., 21823 30th Drive SE, Bothell, WA 98021. Phone: 425-527-4796 Fax: 425-527-4109; E-mail: cneumann@seagen.com

doi: 10.1158/1535-7163.MCT-18-0643

Materials and Methods

Chemicals

FK-866 was purchased from Cayman Chemical. Inhibitors and drug linkers were prepared using standard synthetic chemistry methods as previously described (15); detailed experimental procedures for compounds **2**, **4**, **5**, **8,** and the probe molecule (compound **S12**) used in the fluorescence polarization assay are provided in the Supplementary Methods file. Inhibitors were formulated in DMSO at 10 mmol/L and stored at −20°C. Drug linkers were formulated in dimethylacetamide (DMA) at 20 mmol/L and stored at −20 °C. PBS (pH 7.4) was purchased from Thermo Fisher Scientific (catalog no. 10010-023).

Fluorescence polarization assay

NAMPT bearing a C-terminal His-tag was expressed and purified from *E. coli* as described previously, except a single round of purification using nickel-agarose affinity chromatography was employed (16). Eleven-point, 2-fold serial dilutions of test compounds were prepared in assay buffer (50 mmol/L HEPES, 50 mmol/L KCl, 5 mmol/L $MgCl_2$, 125 μmol/L ATP, 0.005% BSA, 0.5 mmol/L β-mercaptoethanol, pH 7.2) starting at 10 μmol/L (2× final concentration). NAMPT and fluorescent probe molecule **S12** were prepared at 2× final concentrations of 240 nmol/L and 60 nmol/L, respectively, in assay buffer. In black-walled 384-well plates, 15 μL of test compound and 15 μL NAMPT/probe preparations were mixed in quadruplicate and allowed to equilibrate for 4 hours. Fluorescence polarization was measured on an Envision multilabel reader (Perkin Elmer) using an installed FITC FP dual mirror. Measurements of polarization (milli-polarization units) are defined as (mP) = 1,000 × (S-G × P)/(S+G × P) where S and P represent the parallel and perpendicular background subtracted fluorescence count rates following polarized excitation, and G (grating) is an instrument dependent factor calculated from pure fluorophore solution. Binding data were analyzed using GraphPad Prism software using the four-parameter log(inhibitor) versus response model to provide EC_{50} values.

In vitro cytotoxicity assays

The L540cy cell line was provided by Dr. Harald Stein (Institute fur Pathologie, University of Veinikum Benjamin Franklin, Berlin, Germany) and cultured in RPMI1640 with 20% FBS. The A549, HepG2, and Ramos cell lines were obtained from ATCC. The L-428, DOHH-2, and HNT-34 cell lines were obtained from DSMZ. EMEM + 10% FBS was used to culture HepG2 cells; RPMI1640 + 10% FBS was used to culture DOHH-2, HNT-34, L-428, and Ramos cells; F-12K + 10% FBS was used to culture A549 cells. All cell lines were authenticated by short tandem repeat profiling at IDEXX Bioresearch and cultured for no more than 2 months after resuscitation. Cells cultured in log-phase growth were seeded for 24 hours in 96-well plates containing 150 μL RPMI1640 supplemented with 20% FBS. Serial dilutions of antibody–drug conjugates in cell culture media were prepared at 4× working concentrations, and 50 μL of each dilution was added to the 96-well plates in duplicate. Following addition of test articles, cells were incubated with test articles for 4 days at 37°C; for kinetic experiments, cells were incubated for the indicated times (1–5 days). Viability, as indicated by ATP levels, was measured by CellTiter-Glo (Promega). NAD levels were measured using NAD/NADH-Glo (Promega). Luminescence was measured on an Envision Multilabel Reader (Perkin Elmer). The data was analyzed using GraphPad Prism software using the four-parameter log(inhibitor) versus response model to provide EC_{50} values. EC_{50} value for cellular assays is defined here as the concentration that results in 50% reduction in assay signal relative to untreated controls.

Crystallography

NAMPT was crystallized as described previously (17) with the notable exception that large diffraction quality crystals were obtained through a method of microseeding using a cat whisker. NAMPT–inhibitor cocrystals were obtained by soaking the previously grown protein crystals with 2 mmol/L compound **2** for 30 minutes before cryoprotection and flash freezing in liquid nitrogen.

NAMPT compound data were collected at data beamline 4.2.2 at the Advanced Light Source (Lawrence Berkeley Labs). Images were indexed and processed using XDS, and structure solution by the difference Fourier method and refinement were performed using the PHENIX package. Model building was carried out iteratively using the Coot software. Data collection and refinement statistics are given in Supplementary Table S1. The atomic coordinates have been deposited in the Protein Data Bank (www.rcsb.org; PDB ID code 6E68).

Preparation of antibody–drug conjugates

All antibodies used for this study were of the IgG1 isotype. The αCD30 antibody is clone cAC10/brentuximab (18, 19); the αCD19 antibody is clone hBU12/denintuzumab (20, 21); the αCD123* antibody is clone h7G3ec containing an S239C mutation (22). "IgG" denotes a human mAb with no known binding epitope; IgG* is the corresponding antibody with S239C mutation. Reduction of antibody interchain disulfides and disulfide-capped S239C residues was achieved by incubation with an excess of tris(2-carboxyethyl)-phosphine (TCEP) for 60 minutes at 37°C. Reduced mAb was then buffer-exchanged into PBS + 2 mmol/L EDTA using a NAP-5 desalting column (GE Healthcare). Full reduction was confirmed by reverse-phase chromatography (PLRP 3 μm, Agilent; detailed descriptions of all analytic methods are provided in the Supplementary Methods file). Conjugation was carried out at room temperature by adding 1.15 molar equivalents of drug linker per reduced cysteine. After 20 minutes, the extent of conjugation was assessed by evaluating the mass increase of antibody chains using reverse-phased UPLC (PLRP 3 μm, Agilent) coupled with mass spectrometric detection (Waters Xevo G2-S QTOF). Additional drug linker was added when needed. Once all available cysteines were occupied with drug, excess drug-linker was removed by incubation with activated charcoal followed by buffer exchange into PBS using a NAP-5 desalting column. Aggregation was assessed by size-exclusion chromatography. Homogenous drug loading at interchain disulfides, and S239C mutations sites where applicable, was confirmed by comparing predicted and observed changes in the molecular weights of heavy and light chains using PLRP-MS analysis and confirming absence of underloaded species. Characterization data for all ADCs is provided in Supplementary Table S2. Final ADCs were sterile-filtered through a 0.22-μm centrifugal filter and concentration was determined by the DC Protein Assay (Bio-Rad Laboratories).

Plasma stability of ADCs

ADCs were incubated in sterile rat plasma (Sprague Dawley) at 37°C. Time points were collected at 0 hour, 6 hours, 1 day, 3 days, and 7 days. ADC samples were recovered from plasma by batch purification using Anti-Human Capture Affinity Resin (IgSelect, GE Healthcare) for 2 hours. Bound samples were washed with PBS + 0.5 mol/L NaCl and eluted using 50 mmol/L glycine, pH 3. Eluted samples were neutralized with Tris pH 7.4, deglycosylated using PNGase F (New England BioLabs Inc) and reduced using 10 mmol/L DTT. Each sample was analyzed using reverse-phase UPLC (PLRP 3 μm, Agilent) coupled with mass spectrometric detection (Waters Xevo G2-S QTOF). The drug-to-antibody ratio of each sample was calculated using the relative intensity of the deconvoluted masses of the drug-loaded antibody chains and observed peaks indicating decomposition products.

Animal studies

All experiments were conducted in concordance with the Institutional Animal Care and Use Committee in a facility fully accredited by the Association for the Assessment and Accreditation of Laboratory Animal Care.

Pharmacokinetics

Pharmacokinetic studies were performed in naïve female Sprague Dawley rats (Envigo). ADCs with DAR = 8 were evaluated using a radiolabel methodology. To a solution of antibody or ADC in PBS supplemented with an additional 50 mmol/L potassium phosphate (pH 8.0) and 50 mmol/L sodium chloride was added 55 μCi N-succinimidyl propionate, [propionate-2,3-3H]- (Moravek Biochemicals, 80 Ci/mmol, 1 μCi/mL, 9:1 hexane:ethyl acetate solution) per mg of antibody or ADC. The resulting mixture was vortexed and left at room temperature for 2 hours. The mixture was centrifuged at 4,000 × *g* for 5 minutes and the lower aqueous layer was removed. Unconjugated radioactivity was removed by buffer-exchange into PBS using a NAP-5 desalting column followed by one round of dilution and centrifugation at 4,000 × *g* using an Amicon 30-kDa MWCO Ultra-15 Centrifugal Filter Units (Millipore). The resulting products were filtered through sterile 0.22-μm Ultrafree-MC Centrifugal Filter Units (Millipore) and the final antibody or ADC concentration was measured using the DC Protein Assay (Bio-Rad Laboratories). The specific activity (μCi/mg) of each product was determined by liquid scintillation counting.

Test articles were administered at 1 mg/kg via intravenous injection ($n = 3$ per ADC). Blood was drawn into K2EDTA tubes via the saphenous vein at various time points or by cardiac puncture for terminal bleeds. Plasma was isolated by centrifugation for 10 minutes at 10,000 × *g*. A 10–20 μL sample of plasma from each time point was added to 4-mL Ecoscint-A liquid scintillation cocktail (National Diagnostics) and the total radioactivity was measured by liquid scintillation counting. The resulting disintegrations per minute values were converted to μCi and the specific activity of the radiolabeled test articles was used to calculate the concentration of antibody or ADC remaining in the plasma at each time point. The data were fit to a noncompartmental model to derive the clearance rates using Phoenix WinNonLin v7 (Certara).

The IgG*-**8** ADC (DAR = 10) was prepared without radiolabeling. Dosing of ADC and collection of samples was as described above. Total human IgG was detected in plasma using the Gyrolab platform (Gyros AB). Assay standards and quality control samples (QCs) were prepared using IgG*-8 ADC (DAR = 10) diluted in pooled female Sprague Dawley rat plasma. Standards, QCs, and study samples were diluted 10-fold into Rexxip buffer (Gyros AB). Briefly, a biotinylated murine anti-human IgG was captured onto streptavidin-coated beads within the Gyrolab Bioaffy CD. After being captured, human IgG was detected with an Alexa Fluor 647 (Thermo Fisher Scientific) labeled version of the same anti-human IgG. The fluorescence signal (in Response Units) was read at the 1% photomultiplier tube (PMT) setting. Unknown sample concentrations were determined by interpolating against a standard curve fit with a 5-parameter logistic function weighted by $1/y^2$ using the Gyrolab Evaluator Software (Version 3.4.0.24).

In vivo xenograft efficacy models

Tumor cells, as a suspension, were implanted subcutaneously in immunocompromised SCID mice. Upon tumor engraftment, mice were randomized to study groups ($n = 5$) once the average tumor volume reached approximately 100 mm^3. The ADCs were dosed by intraperitoneal injection at indicated times. For the HNT-34 model, animals were dosed with hIgG 24 hours prior to test article administration to reduce Fc-mediated ADC uptake into cells (23). Tumor volume as a function of time was determined using the formula $(L \times W^2)/2$. Animals were euthanized when tumor volumes reached 1,000 mm^3. Complete response (CR) is defined here as absence of measureable mass at tumor site during the course of an experiment.

Intratumoral NAD measurement

NAD measurements in xenografted tumors were obtained using an adaptation of the *in vitro* NAD/NADH-Glo assay. Tumor masses were collected from animals 4 days postdose, cut into portions of approximately 50 mg, and suspended in 1 mL 0.1 mol/L perchloric acid in lysing matrix D vials (MP Biomedicals). The tumors were homogenized in a bead beater using three 30-second cycles, cooling in an ice-water bath in between cycles. Homogenates were centrifuged at 16,000 × *g* for 10 minutes to pellet debris. Supernatant was removed and further diluted 1:5 in 0.1 mol/L perchloric acid. To measure NAD content, 3 μL of diluted tumor lysate was added to 75 μL buffer (0.2 mol/L Tris, pH 7.4) in triplicate, followed by 50 μL NAD/NADH-Glo detection reagent. After 30 to 60 minutes, luminescence was measured on an Envision multilabel reader (Perkin Elmer). NAD concentrations were interpolated from a standard curve of NAD using GraphPad Prism.

Toxicology

In vivo rat safety studies were done in naïve female Sprague Dawley rats (Envigo). Studies had 3 animals/group/timepoint and included a vehicle control group (1× PBS pH 7.4). Animals were administered a single dose of 30, 60, and 100 mg/kg IgG-**8** (DAR = 8) via intravenous injection. Animals were necropsied and tissues were collected at 1 and 4 weeks postdose. Blood was sampled under isoflurane anesthesia via the jugular vein for periodic hematology analysis on the Sysmex XT-2000iV. At necropsy, blood was collected from the caudal vena cava for hematology and clinical chemistry panels and organs were collected for histologic evaluation. Clinical chemistry was analyzed on a Beckman Coulter AU680. The eyes were fixed in modified Davidson solution for 24 hours and transferred to 10% neutral buffered formalin. The remaining organs were fixed in 10% NBF. Tissues were processed routinely into 5-μm thick, hematoxylin and eosin

(H&E)-stained slides for light microscopic evaluation by the same anatomic pathologist.

Results

Identification of linker-compatible NAMPT inhibitors

Development of a cleavable linker for drug release requires the presence of a reactive heteroatom in the drug, typically in the form of an amine, hydroxyl, or sulfhydryl functional group (24–29). FK-866 is devoid of these groups leading us to pursue new linker-compatible analogues (30). The cocrystal structure of FK-866 with NAMPT (16) shows a clearly defined pharmacophore consisting of (i) a heteroaromatic head group which mimics nicotinamide, (ii) a connecting functional group with H-bonding potential, (iii) a hydrophobic extension, and (iv) a "tail" group which makes weak contacts with the entrance to the binding site. Portions of the tail group are largely solvent-exposed, and we rationalized that modifications in this area might yield inhibitors that retain binding potency while incorporating the necessary chemical handle for linker attachment. For this study, a series of FK-866 analogues were prepared consisting of aniline substitutions at different positions on the aromatic tail (Fig. 1, compounds **1–3**). To rank biochemical potency, the analogues were evaluated for binding to NAMPT using a competitive fluorescence polarization (FP) assay where they displayed varying reductions in EC_{50} as compared with FK-866. The compounds were further evaluated for cytotoxicity against L540cy, A549, and HepG2 cell lines. Compound **2** displayed similar potency to FK-866 in both assays. To validate the binding mode of **2**, we prepared crystals of NAMPT with the inhibitor bound (Fig. 1B). The key interactions of the head group pyridine and the acrylamide functional groups seen for FK-866 are maintained (16). Unexpectedly, the newly incorporated aniline group interacts with the backbone amide of Glu376 via a hydrogen bond, potentially offsetting any desolvation penalty for addition of a polar functional group.

Prioritizing the 3-NH_2 modification of the tail group, we next evaluated alternative head groups present within other known NAMPT inhibitors. Analogues of compound **2** were prepared containing the pyridyl-cyanoguanidine group found in the potent inhibitor CHS-828 (31) to give compound **4**, and with a pyridyl-squaramide group (32) to give compound **5**. These head group substitutions similarly retained strong binding to NAMPT in the FP assay and potent cytotoxicity in the cell-based viability assay (Fig. 1).

Preparation of ADCs with NAMPTi payloads

On the basis of the strong potency in biochemical and cell-based assays, compounds **2**, **4**, and **5** were advanced to evaluation as ADC drug payloads using a cleavable linker system (Fig. 2A). To maximize hydrophilicity of the drug linker, we employed a glucuronide trigger, which serves to activate drug release upon cleavage by β-glucuronidase in endosomes and lysosomes (27). For each payload drug, the tail group aniline moiety was joined to the core linker via a carbamate bond, providing a linkage that is chemically stable in plasma but that releases drug rapidly upon cleavage of the glucuronide moiety. Finally, an appended maleimide group provides a handle for bioconjugation to antibodies, with select maleimide formats providing for stabilization of the linkage and/or addition of a polyethylene glycol (PEG) chain to enhance hydrophilicity (33, 34).

A

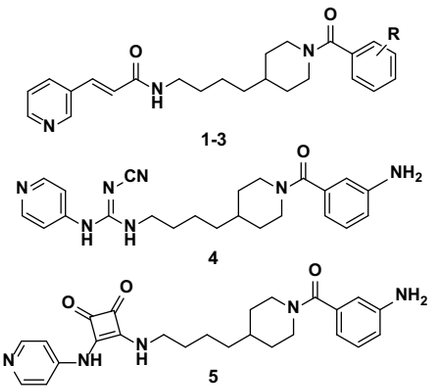

Compound	R	FP assay EC_{50} (nmol/L)	Cell viability EC_{50} (nmol/L) L540cy	A549	HepG2
FK-866	H	38 (35.1–41.1)	6.7 (2.1–21)	25 (19–46)	6.8 (2.7–7.8)
1	2-NH_2	101 (96–107)	9.4 (7.9–21)	–	7.3 (6.3–8.4)
2	3-NH_2	48 (45–51)	6.3 (4.5–8.8)	37 (32–44)	7.6 (1.8–33)
3	4-NH_2	117 (107–128)	–	940 (148–4,800)	–
4	*NA*	32 (29–36)	5.2 (1.8–14.5)	–	5.9 (1.9–17)
5	*NA*	27 (25–29)	12 (8.7–28)	–	14 (11–22)

B

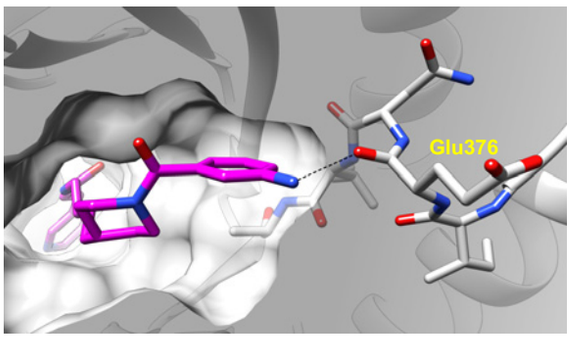

Figure 1.

A, Structures and activities of NAMPT inhibitors as free drugs. EC_{50} value (nmol/L) in FP assay is the concentration required to displace a fluorescently labeled derivative of FK-866 as described in Materials and Methods. Cell viability was determined using CellTiter-Glo following a 96-hour incubation with test article. 95% confidence intervals are indicated in parentheses. **B,** Bound structure of inhibitor **2** showing additional hydrogen bonding from aniline to the backbone amide of Glu376.

Bioconjugation to antibodies was achieved by full reduction of interchain disulfides followed by incubation with the synthetic drug linkers to give ADCs with high degrees of homogeneity having a drug-to-antibody ratio of 8 ("DAR = 8"). In addition to native IgG1 backbones, we examined antibody backbones engineered to include an S239C mutation in the heavy chain (35). Full reduction of these engineered antibodies followed by bioconjugation gave ADCs with a DAR = 10. Both DAR = 8 and DAR = 10 ADCs showed minimal aggregation by SEC (Fig. 2B;

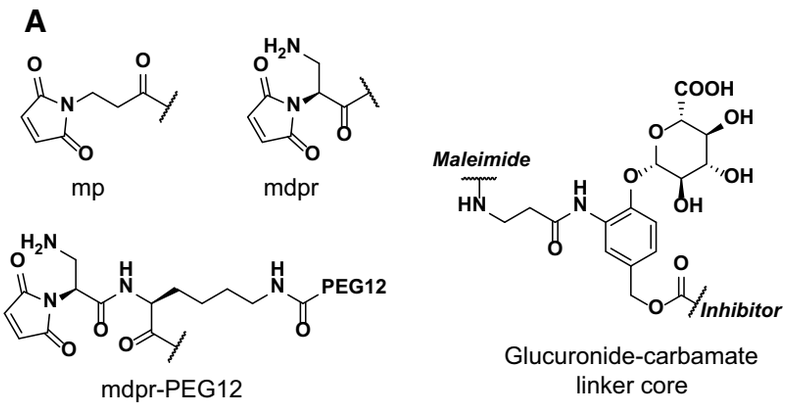

Drug linkers used in this study

Linker ID	Maleimide	Inhibitor
6	mp	**4**
7	mp	**5**
8	mdpr	**2**
9	mdpr-PEG12	**2**

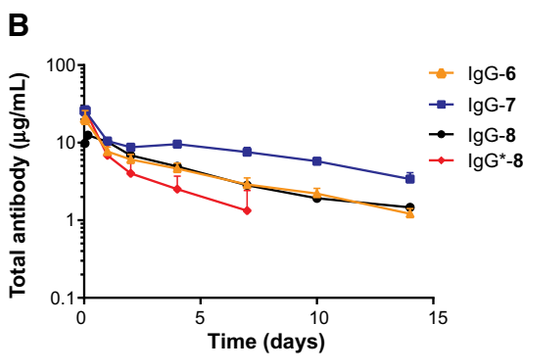

ADC	DAR	Aggregation (%)	$T_{1/2}$ (d)	AUC_{inf} (day*µg/mL)
IgG-**6**	8	1.1	6.4	65.1
IgG-**7**	8	1.5	5.2	137
IgG-**8**	8	2.9	7.6	72.5
IgG*-**8**	10	1.2	2.5	39.7

Figure 2.

A, Chemical structures of drug linker components and description of linkers used herein. Core structure of linker identifies location of maleimide and inhibitor attachment sites. All inhibitors were connected to linker core through the tail-group aniline functionality. **B,** Pharmacokinetic profile of ADCs in Sprague Dawley rats. Data points indicate mean ± SD and graphing is suspended if any measurement in a group falls below the lower limit of quantitation. Aggregation represents percent of high-molecular weight species in test article preparation as determined by SEC. Pharmacokinetic parameters were derived from experimental data using a noncompartmental model.

Supplementary Table S2). An isotype control ADC using linker **8**, containing the self-stabilizing mdpr maleimide, was evaluated for stability upon incubation in rat plasma. Over an 8-day incubation, there was no observed payload loss resulting from carbamate cleavage or linker loss resulting from deconjugation (Supplementary Fig. S1). Pharmacokinetic analyses nonbinding ADCs carrying linkers **6**–**8** (DAR = 8) were carried out in rats at a dose of 1 mg/kg and showed terminal half-lives in the range of 5–8 days, similar to other ADCs in clinical use (36, 37). A DAR = 10 ADC using linker **8** displayed a reduced terminal half-life of 2.5 days, but after one week still maintained plasma concentrations above the EC_{50} values determined in *in vitro* assays (see below). The chemical stability and pharmacokinetic profiles of these ADC formats met our criteria for further preclinical evaluation.

In vitro activity of NAMPTi-ADCs

To evaluate biological activity of NAMPT inhibitors delivered as ADCs, we prepared conjugates of candidate linkers using an anti-CD30 antibody. The conjugates were evaluated for activity using two *in vitro* assay formats (Fig. 3A). In the first, NAD levels were measured providing a direct evaluation of the pharmacodynamic effect of the conjugates. In addition, ADCs were tested in a standard viability assay that measures ATP content as a surrogate for viability. In the L540cy cell line, a model of CD30-positive Hodgkin lymphoma, all three ADCs displayed effective depletion of NAD and ATP. Immunologic specificity of the conjugates was established with HepG2, a hepatocellular carcinoma cell line that is sensitive to NAMPT inhibition but lacks CD30 expression thereby rendering it insensitive to the ADCs in both assay formats.

Because literature precedents suggest that sustained NAD depletion is required for progression to cell death (8, 38, 39), we investigated the temporal aspects of NAD and ATP depletion following ADC treatment. L540cy cells were treated with αCD30-**8** and assayed for NAD and ATP levels every 24 hours over five days (Fig. 3B; Supplementary Fig. S2). Two trends in the data were noteworthy. First, doses above the 96-hour EC_{50} led to substantial decline in NAD (~10% of untreated) within 24 hours, while ATP levels did not fall below 50% until 72 hours. This delay between NAD and ATP depletion likely reflects a reserve of ATP equivalents that can sustain energy metabolism through transient NAD depletion. Second, we observed that doses of ADC just below the 96-hour EC_{50} led to initial depletion of NAD at 24 hours, but that levels are restored at later time points and no downstream effect on ATP levels results. This behavior results in a steepening of dose–response curves over time (Supplementary Fig. S2), and suggests that NAD levels must fall below a certain threshold to disrupt ATP synthesis and elicit cell death. While these kinetic and threshold behaviors have been reported for free NAMPT

A

ADC	DAR	L540cy (CD30+) NAD	L540cy (CD30+) ATP	HepG2 (CD30-) NAD	HepG2 (CD30-) ATP
αCD30-6	8	9 ng/mL (2.7–27)	13 (11–16)	>2,000	>2,000
αCD30-7	8	29 (18–40)	50 (40–76)	>2,000	>2,000
αCD30-8	8	9 (5–22)	39 (33–67)	>2,000	>2,000

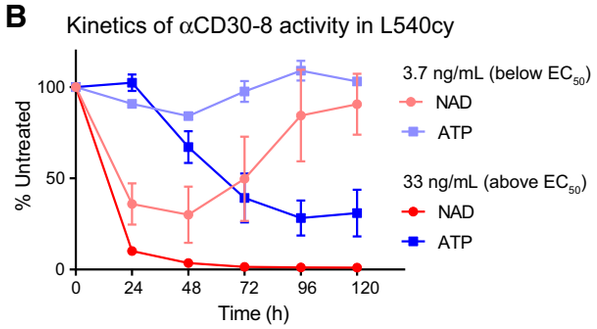

Figure 3.

A, *In vitro* EC_{50} values (ng/mL) for αCD30-ADCs in assays of NAD depletion (NAD/NADH-Glo) and ATP depletion (CellTiter-Glo). 95% confidence intervals are indicated in parentheses. Cells were incubated with test article for 96 hours prior to measurement. Strong NAD- and ATP-depleting activity is observed on CD30-positive L540cy cells, while no activity is observed in CD30-negative HepG2 cells. **B,** Timecourse of NAD and ATP depletion by αCD30-**8** in L540cy cells. At 3.7 ng/mL (below the 96-hour EC_{50}), NAD levels decrease initially but recover by 120 hours while ATP levels are unchanged. At 33 ng/mL (above the 96-hour EC_{50}), NAD levels remain low over time and ATP levels drop after approximately 48–72 hours.

inhibitors, we confirm these apply to ADC delivery and suggest they may be relevant to appropriate application of the platform.

In vivo activity of NAMPTi-ADCs

To investigate the pharmacodynamic effect of NAMPTi-ADCs *in vivo*, we measured intratumoral NAD levels in mice bearing L540cy Hodgkin lymphoma xenografts (Fig. 4A). For our initial *in vivo* studies, we employed linker **9**, which includes a hydrophilic PEG with the potential to maximize pharmacokinetic half-life (33). SCID mice bearing subcutaneous xenografts were treated with αCD30-**9** at doses of 3 mg/kg and 10 mg/kg. At 4 days postdose, tumors were excised, homogenized, and assayed for NAD content using an adaptation of the *in vitro* NAD assay. In untreated tumors, NAD was detected at a concentration of 35–110 μg/g tissue. In tumors treated at either dose, NAD was detected at or near the assay background, thus demonstrating that the ADCs maintain their pharmacodynamic effect *in vivo*.

Tumor-regressing activity of αCD30-**9** was further evaluated in the L540cy xenograft model at doses of 1, 3, and 10 mg/kg. In congruence with the pharmacodynamic data, single doses of 3 and 10 mg/kg led to complete tumor regressions in all animals, with only a single animal dosed at 3 mg/kg experiencing tumor outgrowth after 65 days (Fig. 4B). Mice treated at 1 mg/kg showed tumor growth delay but no complete regressions. Also evaluated in this efficacy experiment was αCD30-**8**, where drug linker **8** differs from **9** by absence of the hydrophilic PEG moiety; both

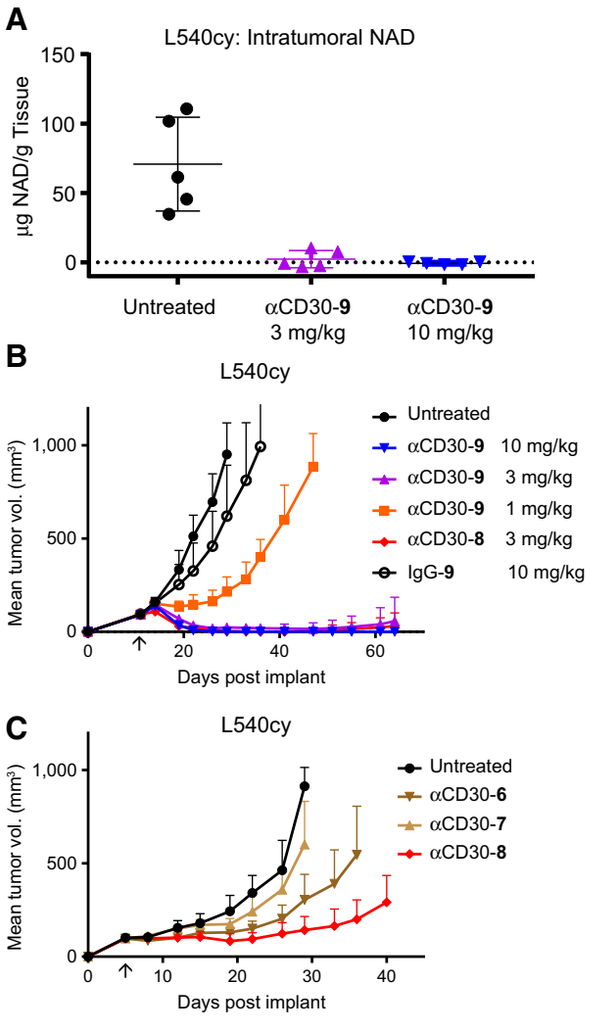

Figure 4.

In vivo activity of αCD30-ADCs in L540cy xenografts. **A,** NAD content (μg NAD/g tissue) measured in tumors 4 days after administration of αCD30-**9**. Each point represents the mean of three technical replicates for an individual animal. Bars indicate mean ± SD of the group. **B,** Dose response for efficacy of αCD30-**9**. Plotting of data for a specific group ends when the first animal was euthanized (tumor volume >1,000 mm^3) or at the end of the study (day 64). At the end of the study complete responses were maintained for 5/5 animals in the 10 mg/kg dose group and 4/5 animals in the 3 mg/kg dose group. One animal in the 3 mg/kg dose group achieved a complete response during the study, but tumor regrowth resumed before day 64. The αCD30-**8** ADC lacking a PEG linker element showed equivalent activity to αCD30-**9** (3 mg/kg dose, 4/5 CR at day 64) indicating that the PEG moiety does not enhance *in vivo* efficacy of the ADCs. **C,** Comparison of αCD30-ADCs carrying different NAMPT inhibitor payloads. Subcurative dosing at 1 mg/kg allows identification of linker **8** as the more efficacious drug linker.

linkers lead to the intracellular release of inhibitor **2**. Because both ADCs showed equivalent activity at 3 mg/kg, we prioritized linker **8** over linker **9** for further study due to its simplified chemical structure and favorable pharmacokinetic properties.

The relative efficacy of the three prioritized payloads containing different head group structures was also compared in the L540cy xenograft model. Anti-CD30 ADCs bearing drug linkers **6**, **7**, and **8**

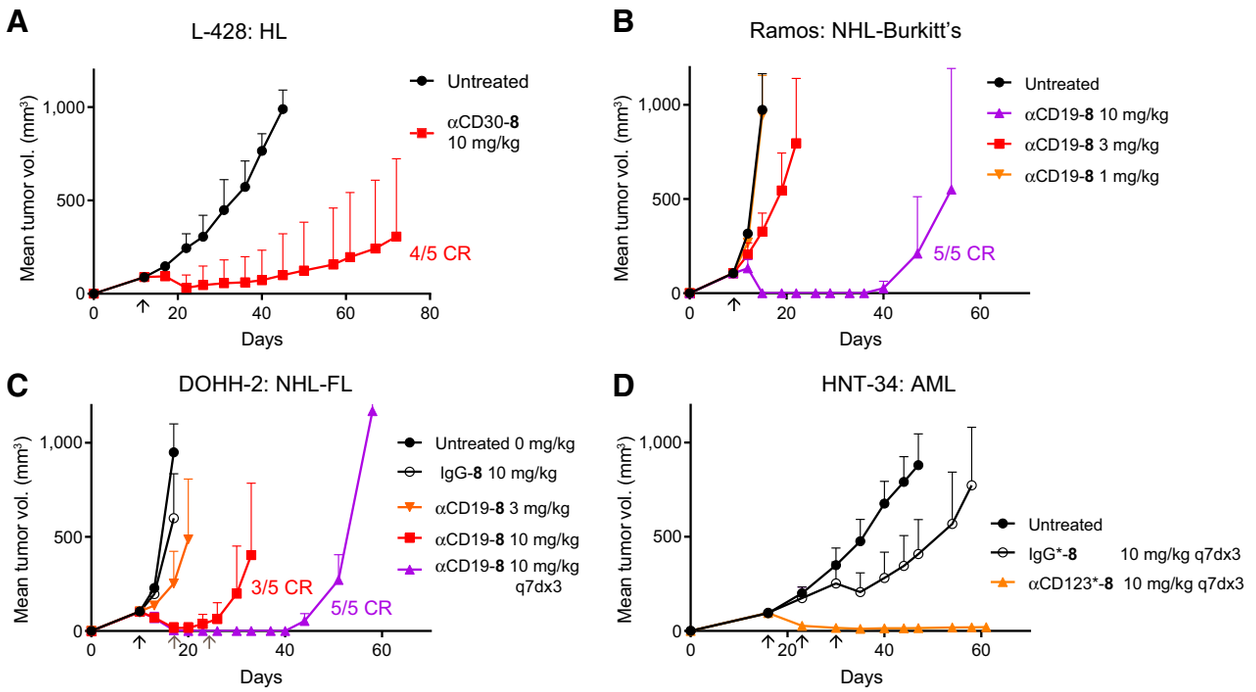

Figure 5.

Evaluation of drug linker **8** in additional xenograft models. Plots indicate mean tumor volume + SD. **A,** Treatment of CD30$^+$ L-428 (Hodgkin lymphoma) tumor xenograft with a single 10 mg/kg dose (arrow) of αCD30-**8** results in 4 of 5 complete responses. **B** and **C,** Treatment of CD19$^+$ Ramos (Burkitt lymphoma) and DOHH-2 (follicular lymphoma) xenografts with a single 10 mg/kg dose of αCD19-**8** (black arrows) results in 5 of 5 and 3 of 5 complete responses, respectively. Additional weekly dosing in DOHH-2 (gray arrows) increases the CR rate and extends the durability of response. **D,** Treatment of CD123$^+$ HNT-34 (acute myeloid leukemia) xenografts with three weekly doses of αCD123*-**8** (DAR 10; arrows) at 10 mg/kg results in significant tumor regression. The study was ended when residual palpable mass was deemed to be nonviable.

were administered at the subcurative dose of 1 mg/kg. Despite comparable *in vitro* activities, αCD30-8 provided the greatest tumor growth delay (Fig. 4C).

To understand the breadth of activity of NAMPTi-ADCs, additional xenograft models for Hodgkin lymphoma, non-Hodgkin lymphoma, and acute myeloid leukemia were evaluated using ADCs targeting CD30, CD19, and CD123, respectively (Fig. 5). *In vitro* NAD and ATP depletion assays were performed in the selected cell lines with the ADCs prior to xenograft studies (Supplementary Table S3). Interestingly, while all the ADCs demonstrated good activity in the NAD assay, none were able to achieve an EC_{50} value in the ATP assay.

In the CD30-positive L428 xenograft model, a single dose of αCD30-**8** at 10 mg/kg resulted in complete tumor regressions in 4 of 5 treated mice (Fig. 5A). For NHL, the Ramos (Burkitt lymphoma) and DOHH2 (follicular lymphoma) models were selected for evaluation *in vivo* using αCD19-**8**. In Ramos, single doses of αCD19-**8** at 10 mg/kg gave complete regressions in all animals treated (Fig. 5B). In DOHH2, complete regressions were observed in 3 of 5 mice treated with a single dose of 10 mg/kg (Fig. 5C). Because of the shorter duration of these responses, we extended dosing in this model to 3 weekly doses (q7dx3) of 10 mg/kg ADC and observed complete regressions in all animals with greatly extended durability of response. For AML, the HNT-34 xenograft was evaluated with αCD123*-**8** (DAR = 10) using the 10 mg/kg q7dx3 dosing regimen (Fig. 5D). The isotype control ADC IgG*-**8** (DAR = 10) showed a transient interruption of tumor growth following the third dose, potentially driven by the ability of AML cells to uptake ADCs via Fc-mediated interactions (23). In contrast, αCD123*-**8** induced rapid tumor regression after the initial dose and sustained tumor regression after subsequent doses. Taken together, these various models indicate that the NAMPTi payload can be efficacious in multiple tumor indications when delivered with antibodies that bind various tumor antigens.

Toxicology

In single-dose rat toxicity studies, administration of the IgG-**8** ADC was well tolerated at the tested doses of 30, 60, and 100 mg/kg. Toxicities associated with the ADC included acute decreases in circulating lymphocytes, monocytes, eosinophils, red blood cells (RBC) and reticulocytes on study days 4 and 8, with no reduction in platelets (Fig. 6A). There were no significant changes in serum chemistry parameters. The timing of the RBC and reticulocyte nadir (study day 4 and 8, respectively) and histologic appearance of increased pigment (presumed hemosiderin) in the spleen is suggestive of an extravascular hemolytic component (Fig. 6B). Investigations are ongoing to determine the mechanism of this toxicity as well as its translatability between species. Spleenic red pulp hyperplasia and extramedullary hematopoiesis seen at one week post dose are likely compensatory in response to the anemia. Both the test article and physiologic stress likely contributed to the lymphoid depletion present in the lymph nodes, spleen, and thymus.

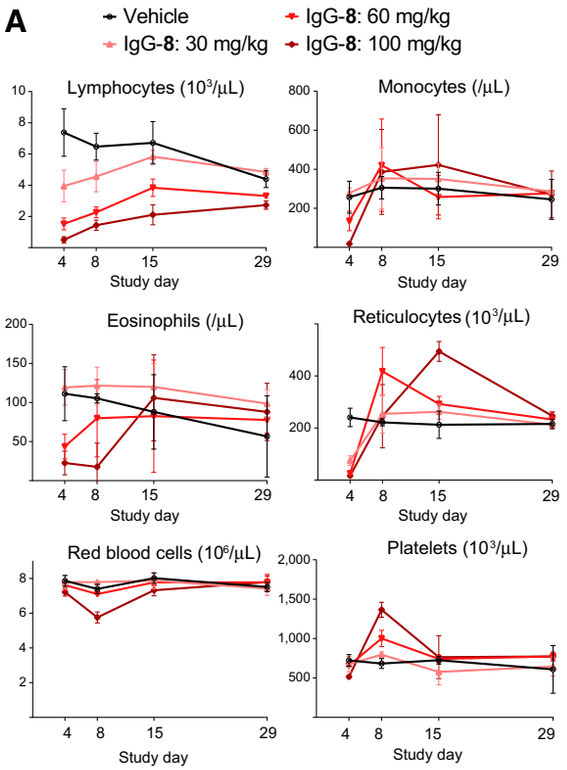

B

Histopathology (study day 4)‡

Organ	Finding		IgG-8 30 mg/kg	IgG-8 60 mg/kg	IgG-8 100 mg/kg
Liver	Within normal limits		3/3	3/3	0/3
	Extramedullary hematapoeisis	-Minimal	0/3	0/3	3/3
Lymph nodes, mesenteric	Within normal limits		3/3	3/3	0/3
	Lymphod depletion	-Minimal	0/3	0/3	3/3
Spleen	Within normal limits		3/3	3/3	0/3
	Lymphoid depletion	-Mild	0/3	0/3	3/3
	Red pulp hyperplasia	-Minimal	0/3	0/3	1/3
		-Mild	0/3	0/3	1/3
	Macrophage pigment accumulation	-Minimal	0/3	0/3	1/3
		-Mild	0/3	0/3	1/3
Thymus	Within normal limits		0/3	0/3	0/3
	Lymphoid depletion	-Mild	2/3	0/3	0/3
		-Moderate	1/3	0/3	1/3
		-Severe	0/3	3/3	2/3
Eye	Within normal limits		3/3	3/3	3/3
Heart	Within normal limits		3/3	3/3	3/3

‡All findings were reversed by study day 29

Figure 6.

A, Hematology counts in Sprague Dawley rats after intravenous administration of a single dose of non-binding ADC IgG-**8**. Individual points represent mean ± SD. Initial declines in lymphocytes, monocytes, eosinophils, reticulocytes, and red blood cells are recovered by study day 29 (4 weeks postdose). Platelet counts do not decline following treatment, consistent with the absence of thrombocytopenia induced by systemic administration of NAMPT inhibitors to rodents. **B,** Acute (study day 4) histopathology findings in all dose groups. All findings were within normal limits upon terminal necropsy.

All findings from hematology and histopathology recovered by study day 29 (4 weeks postdose). In contrast to reports for NAMPT inhibitor small molecules, neither myocardial nor retinal toxicities were evident in the rat toxicity studies (12, 13).

Discussion

While NAMPT inhibitors are potent cytotoxic molecules, their utility as chemotherapeutic agents in the treatment of cancer has been hampered by toxicity. In this work, we introduce NAMPT inhibitors as a viable drug class for targeted delivery to cancer cells using ADCs.

Structure-guided modification of the prototypical inhibitor FK-866 allowed the identification of new inhibitors, which retained cytotoxic activity in cells and possessed a chemical handle on which to attach an enzyme-cleavable drug linker. Candidate payloads were prioritized as free drugs based on a biochemical binding assay against NAMPT followed by a viability assay using a small panel of cell lines. Three select inhibitors were advanced to drug linker synthesis using a glucuronide-based linker system to maximize the hydrophilic character of the molecules. Ultimately, the combination of payload and linker chemistry delivered ADCs with excellent biophysical properties. Negligible aggregation was observed with ADCs conjugated with 8 or 10 drug equivalents, and pharmacokinetic analysis in rats confirmed favorable exposure and clearance parameters consistent with advanced ADCs.

From an activity standpoint, the resulting ADCs showed antigen-specific NAD-depleting activity *in vitro*. Secondary ATP-depleting activity is often, but not always, observed *in vitro* (Fig. 2; Supplementary Table S1). The weak or absent ATP depletion in some cell lines after 96 hours of treatment may be due to the kinetics of ADC internalization and drug release. This hypothesis is supported by the observation that application of free NAMPT inhibitors to cells readily leads to complete ATP depletion within a 96-hour experiment. In addition, we postulate that unknown metabolic parameters may influence the potential of a cell line to demonstrate ATP depletion *in vitro*. Ongoing studies in our laboratories are aimed at better understanding the determinants of drug sensitivity in different cell lines.

We further observed that insufficient depletion of NAD at early time points can lead to recovery of NAD levels at later time points (Fig. 3B). The mechanism of this rebound effect is unclear, but the findings suggest that rapid and sustained exposure to drug may be necessary for optimal activity. ADC delivery might thus provide an optimal format for NAMPT inhibition, as the long circulating half-lives of ADCs *in vivo* may provide continual exposure of drug to antigen-positive target cells. At the same time, antigens with high surface expression and/or efficient internalization may provide optimal targets for NAMPTi-ADCs by providing faster intracellular drug exposure and metabolite depletion at the outset of treatment.

The *in vivo* antitumor activity of NAMPTi-ADCs is demonstrated in multiple xenograft models of Hodgkin lymphoma, non-Hodgkin lymphoma, and acute myeloid leukemia. Tumor regressing activity is observed at single doses as low as 3 mg/kg in the L540cy model of Hodgkin lymphoma through CD30-mediated targeting (Fig. 4). In other models of Hodgkin lymphoma, non-Hodgkin lymphoma, and acute myeloid leukemia, tumor regression is commonly observed with a single ADC dose of 10 mg/kg, while a weekly dosing regimen can greatly extend the durability of regressions (Fig. 5). *In vivo* activity of the ADCs roughly parallels the *in vitro* NAD-depleting activity of the ADCs. Weak or absent activity in the ATP depletion assay, a common surrogate for cell viability, does not preclude success in the corresponding xenograft model. This divergence between ATP depletion *in vitro* and xenograft activity may be explained by the temporal aspects of metabolite depletion described for the *in vitro* assays, or alternatively by changes in sensitivity to metabolic disruption as cells experience an altered nutrient environment in a tumor as compared with cell culture media. From a practical standpoint, the better predictive value of the NAD depletion assay supports its routine application as a screening tool in a preclinical development program for NAMPT inhibitor payloads, as exclusive reliance on more traditional ATP-based viability assays may lead to exclusion of active ADCs.

In addition to establishing *in vivo* activity for this class of ADC payloads, a meaningful advance toward a therapeutic can only come with an improvement in the toxicity profile relative to systemic administration of NAMPT inhibitors. Our toxicology data in rodent models indicate that targeted delivery has the potential to improve the therapeutic index. Whereas the tumor-regressing activity of targeted ADCs is typically observed at single doses of 10 mg/kg in our models, single doses of a nontargeted ADC at 100 mg/kg are well tolerated in rats. While mild, dose-dependent cytopenias are observed in acute-phase hematologic and histopathologic evaluations, all findings are recoverable 4 weeks posttreatment (Fig. 6).

Absent from our toxicologic findings are retinal and cardiac degeneration. These toxicities are prominent in rodents and are considered to be class-specific and relevant to the use of NAMPT inhibitors in people. While published data on FK-866 rodent toxicities is limited, comparison of our ADC platform to the small-molecule NAMPT inhibitor GNE-617 is instructive. GNE-617 achieves tumor regression in a U251 glioblastoma xenograft model when dosed at 25 mg/kg orally qdx7, and in additional models when dosed at 10 mg/kg twice daily for 7 days (40, 41). In toxicology studies using SD rats, GNE-617 dosed at 30 mg/kg orally once daily resulted in early animal deaths or euthanasia on study day 4 resulting from myocardial degeneration (12). Retinal degeneration was also observed in this time frame (13). While lower doses of GNE-617 were not reported, these data suggest that efficacious dosing regimens in mouse xenograft models are not well tolerated in the rat model for toxicity. In contrast, the ADC delivery approach shown here achieved tumor regressions at single doses of 10 mg/kg, which is less than 1/10th the MTD in rats (>100 mg/kg). This is in stark contrast to results obtained with GNE-617. Absent from the current characterization of toxicity is thrombocytopenia, a potential dose-limiting toxicity in humans that does not recapitulate in rodent models (9, 42). Understanding of the impact of NAMPTi-ADCs on human platelet biogenesis and survival is a continuing aim of ongoing investigations.

In summary, we have introduced NAMPT inhibitors as novel payloads for ADC technology. Targeted delivery of this drug class provides tumor-regressing activity in multiple xenograft models and a promising therapeutic index in preclinical species. The NAMPTi mechanism of action is distinct from existing ADC payload classes and FDA-approved drugs, starving hyperproliferative cells of an essential metabolic intermediate and inducing a proinflammatory cell death pathway. Continued evaluation of NAMPTi-ADCs in a range of indications is warranted to leverage these unique features in the continued pursuit of therapeutics for clinical application.

Disclosure of Potential Conflicts of Interest

No potential conflicts of interest were disclosed.

Authors' Contributions

Conception and design: C.S. Neumann, K.C. Olivas, P.D. Senter
Development of methodology: L.V. Loftus, P.G. Pittman
Acquisition of data (provided animals, acquired and managed patients, provided facilities, etc.): C.S. Neumann, K.C. Olivas, M.E. Anderson, J.H. Cochran, S. Jin, L.V. Loftus, D.W. Meyer, J.C. Nix, P.G. Pittman, M.L. Ulrich, A.B. Waight, A. Wong, M.C. Zaval, W. Zeng
Analysis and interpretation of data (e.g., statistical analysis, biostatistics, computational analysis): C.S. Neumann, K.C. Olivas, J.H. Cochran, F. Li, L.V. Loftus, J. Neale, J.C. Nix, J.K. Simmons, A.B. Waight, M.C. Zaval
Writing, review, and/or revision of the manuscript: C.S. Neumann, K.C. Olivas, J.H. Cochran, L.V. Loftus, J.K. Simmons, P.D. Senter
Administrative, technical, or material support (i.e., reporting or organizing data, constructing databases): D.W. Meyer, P.G. Pittman
Study supervision: C.S. Neumann, M.E. Anderson, F. Li, J.K. Simmons, R.P. Lyon

The costs of publication of this article were defrayed in part by the payment of page charges. This article must therefore be hereby marked *advertisement* in accordance with 18 U.S.C. Section 1734 solely to indicate this fact.

Received June 20, 2018; revised July 24, 2018; accepted September 14, 2018; published first September 21, 2018.

References

1. Beck A, Goetsch L, Dumontet C, Corvaia N. Strategies and challenges for the next generation of antibody-drug conjugates. Nat Rev Drug Discov 2017; 16:315–37.
2. Ocean AJ, Starodub AN, Bardia A, Vahdat LT, Isakoff SJ, Guarino M, et al. Sacituzumab govitecan (IMMU-132), an anti-Trop-2-SN-38 antibody-drug conjugate for the treatment of diverse epithelial cancers: safety and pharmacokinetics. Cancer 2017;123:3843–54.
3. Lambert JM, Morris CQ. Antibody–Drug Conjugates (ADCs) for personalized treatment of solid tumors: a review. Adv Ther 2017;34:1015–35.
4. Ogitani Y, Aida T, Hagihara K, Yamaguchi J, Ishii C, Harada N, et al. DS-8201a, A novel HER2-targeting ADC with a novel DNA Topoisomerase I inhibitor, demonstrates a promising antitumor efficacy with differentiation from T-DM1. Clin Cancer Res 2016;22:5097–108.
5. Chari RVJ, Miller ML, Widdison WC. Antibody–drug conjugates: an emerging concept in cancer therapy. Angew Chem Int Ed 2014;53:3796–827.
6. Sampath D, Zabka TS, Misner DL, O'Brien T, Dragovich PS. Inhibition of nicotinamide phosphoribosyltransferase (NAMPT) as a therapeutic strategy in cancer. Pharmacol Ther 2015;151:16–31.
7. Cantó C, Menzies Keir J, Auwerx J. NAD+ Metabolism and the control of energy homeostasis: a balancing act between mitochondria and the nucleus. Cell Metabolism 2015;22:31–53.
8. Del Nagro C, Xiao Y, Rangell L, Reichelt M, O'Brien T. Depletion of the central metabolite NAD leads to oncosis-mediated cell death. J Biol Chem 2014;289:35182–92.
9. Holen K, Saltz LB, Hollywood E, Burk K, Hanauske AR. The pharmacokinetics, toxicities, and biologic effects of FK866, a nicotinamide

adenine dinucleotide biosynthesis inhibitor. Invest New Drugs 2008; 26:45–51.
10. Hovstadius P, Larsson R, Jonsson E, Skov T, Kissmeyer AM, Krasilnikoff K, et al. A phase I study of CHS 828 in patients with solid tumor malignancy. Clin Cancer Res 2002;8:2843–50.
11. Pishvaian MJ, Marshall JL, Hwang JJ, Malik S, He AR, Deeken JF, et al. A phase I trial of GMX1777, an inhibitor of nicotinamide phosphoribosyl transferase (NAMPRT), given as a 24-hour infusion. J Clin Oncol 2009;27: 3581.
12. Misner DL, Kauss MA, Singh J, Uppal H, Bruening-Wright A, Liederer BM, et al. Cardiotoxicity associated with nicotinamide phosphoribosyltransferase inhibitors in rodents and in rat and human-derived cells lines. Cardiovasc Toxicol 2017;17:307–18.
13. Zabka TS, Singh J, Dhawan P, Liederer BM, Oeh J, Kauss MA, et al. Retinal toxicity, *in vivo* and *in vitro*, associated with inhibition of nicotinamide phosphoribosyltransferase. Toxicol Sci 2015;144:163–72.
14. Karpov AS, Abrams T, Clark S, Raikar A, D'Alessio JA, Dillon MP, et al. Nicotinamide phosphoribosyltransferase inhibitor as a novel payload for antibody–drug conjugates. ACS Med Chem Lett 2018;9:838–42.
15. Neumann CS, Olivas K, inventors; Seattle Genetics, Inc, assignee. Targeted delivery of nicotinamide adenine dinucleotide salvage pathway inhibitors. United States patent WO/2018/75600. 2018 Apr 26.
16. Khan JA, Tao X, Tong L. Molecular basis for the inhibition of human NMPRTase, a novel target for anticancer agents. Nat Struct Mol Biol 2006; 13:582–8.
17. Wang W, Elkins K, Oh A, Ho YC, Wu J, Li H, et al. Structural basis for resistance to diverse classes of NAMPT inhibitors. PLoS One 2014;9: e109366.
18. Wahl AF, Klussman K, Thompson JD, Chen JH, Francisco LV, Risdon G, et al. The anti-CD30 monoclonal antibody SGN-30 promotes growth arrest and DNA fragmentation *in vitro* and affects antitumor activity in models of Hodgkin's disease. Cancer Res 2002;62:3736–42.
19. The full sequence of cAC10/brentuximab is disclosed in: proposed international nonproprietary names: list 103. WHO Drug Inform 2010;24: 125–98.
20. Gerber H-P, Kung-Sutherland M, Stone I, Morris-Tilden C, Miyamoto J, McCormick R, et al. Potent antitumor activity of the anti-CD19 auristatin antibody drug conjugate hBU12-vcMMAE against rituximab-sensitive and -resistant lymphomas. Blood 2009;113:4352–61.
21. The full sequence of hBU12/denintuzumab is disclosed in: Proposed International Nonproprietary Names: List 111. WHO Drug Inform 2014;28:211–94.
22. Li F, Sutherland MK, Yu C, Walter RB, Westendorf L, Valliere-Douglass J, et al. Characterization of SGN-CD123A, a potent CD123-directed antibody–drug conjugate for acute myeloid leukemia. Mol Cancer Ther 2018; 17:554–64.
23. Boghaert ER, Khandke K, Sridharan L, Armellino D, Dougher M, Dijoseph JF, et al. Tumoricidal effect of calicheamicin immuno-conjugates using a passive targeting strategy. Int J Oncol 2006;28:675–84.
24. Kolakowski RV, Haelsig KT, Emmerton KK, Leiske CI, Miyamoto JB, Cochran JH, et al. The methylene alkoxy carbamate selfimmolative unit: utilization for the targeted delivery of alcoholcontaining payloads with antibody–drug conjugates. Angew Chem Int Ed 2016;55:7948–51.
25. Dubowchik GM, Firestone RA, Padilla L, Willner D, Hofstead SJ, Mosure K, et al. Cathepsin B-labile dipeptide linkers for lysosomal release of doxorubicin from internalizing immunoconjugates: model studies of enzymatic drug release and antigen-specific in vitro anticancer activity. Bioconj Chem 2002;13:855–69.
26. Burke PJ, Hamilton JZ, Pires TA, Setter JR, Hunter JH, Cochran JH, et al. Development of novel quaternary ammonium linkers for antibody–drug conjugates. Mol Cancer Ther 2016;15:938–45.
27. Jeffrey SC, Andreyka JB, Bernhardt SX, Kissler KM, Kline T, Lenox JS, et al. Development and properties of β-glucuronide linkers for monoclonal antibody−drug conjugates. Bioconj Chem 2006;17:831–40.
28. Dokter W, Ubink R, van der Lee M, van der Vleuten M, van Achterberg T, Jacobs D, et al. Preclinical profile of the HER2-targeting ADC SYD983/SYD985: introduction of a new duocarmycin-based linker-drug platform. Mol Cancer Ther 2014;13:2618–29.
29. Widdison WC, Wilhelm SD, Cavanagh EE, Whiteman KR, Leece BA, Kovtun Y, et al. Semisynthetic maytansine analogues for the targeted treatment of cancer. J Med Chem 2006;49:4392–408.
30. Hasmann M, Schemainda I. FK866, a highly specific noncompetitive inhibitor of nicotinamide phosphoribosyltransferase, represents a novel mechanism for induction of tumor cell apoptosis. Cancer Res 2003;63: 7436–42.
31. Schou C, Ottosen ER, Petersen HJ, Björkling F, Latini S, Hjarnaa PV, et al. Novel cyanoguanidines with potent oral antitumour activity. Bioorg Med Chem Lett 1997;7:3095–100.
32. Christensen MK, Erichsen KD, Olesen UH, Tjornelund J, Fristrup P, Thougaard A, et al. Nicotinamide phosphoribosyltransferase inhibitors, design, preparation, and structure-activity relationship. J Med Chem 2013;56:9071–88.
33. Lyon RP, Bovee TD, Doronina SO, Burke PJ, Hunter JH, Neff-LaFord HD, et al. Reducing hydrophobicity of homogeneous antibody-drug conjugates improves pharmacokinetics and therapeutic index. Nat Biotechnol 2015;33:733–5.
34. Lyon RP, Setter JR, Bovee TD, Doronina SO, Hunter JH, Anderson ME, et al. Self-hydrolyzing maleimides improve the stability and pharmacological properties of antibody-drug conjugates. Nat Biotechnol 2014;32:1059–62.
35. Sussman D, Westendorf L, Meyer DW, Leiske CI, Anderson M, Okeley NM, et al. Engineered cysteine antibodies: an improved antibody-drug conjugate platform with a novel mechanism of drug-linker stability. Protein Eng Des Sel 2018;31:47–54.
36. Poon KA, Flagella K, Beyer J, Tibbitts J, Kaur S, Saad O, et al. Preclinical safety profile of trastuzumab emtansine (T-DM1): mechanism of action of its cytotoxic component retained with improved tolerability. Toxicol Appl Pharmacol 2013;273:298–313.
37. Kamath AV, Iyer S. Preclinical pharmacokinetic considerations for the development of antibody drug conjugates. Pharm Res 2015;32: 3470–9.
38. Tan B, Young DA, Lu ZH, Wang T, Meier TI, Shepard RL, et al. Pharmacological inhibition of nicotinamide phosphoribosyltransferase (NAMPT), an enzyme essential for NAD+ biosynthesis, in human cancer cells: metabolic basis and potential clinical implications. J Biol Chem 2013;288:3500–11.
39. Watson M, Roulston A, Belec L, Billot X, Marcellus R, Bedard D, et al. The small molecule GMX1778 is a potent inhibitor of NAD+ biosynthesis: strategy for enhanced therapy in nicotinic acid phosphoribosyltransferase 1-deficient tumors. Mol Cell Biol 2009;29:5872–88.
40. O'Brien T, Oeh J, Xiao Y, Liang X, Vanderbilt A, Qin A, et al. Supplementation of nicotinic acid with NAMPT inhibitors results in loss of in vivo efficacy in NAPRT1-deficient tumor models. Neoplasia 2013;15: 1314–29.
41. Zheng X, Bauer P, Baumeister T, Buckmelter AJ, Caligiuri M, Clodfelter KH, et al. Structure-based discovery of novel amide-containing nicotinamide phosphoribosyltransferase (nampt) inhibitors. J Med Chem 2013;56: 6413–33.
42. Tarrant JM, Dhawan P, Singh J, Zabka TS, Clarke E, DosSantos G, et al. Preclinical models of nicotinamide phosphoribosyltransferase inhibitor-mediated hematotoxicity and mitigation by co-treatment with nicotinic acid. Toxicol Mech Methods 2015;25:201–11.